










## Article

# Approaching the Attosecond Frontier of Dynamics in Matter with the Concept of X-ray Chronoscopy

Wojciech Błachucki <sup>1,\*</sup> , Anna Wach <sup>1</sup> , Joanna Czapla-Masztafiak <sup>1</sup> , Mickaël Delcey <sup>2</sup> , Christopher Arrell <sup>3</sup>, Rafał Fanselow <sup>1</sup> , Pavle Juranić <sup>3</sup>, Marcus Lundberg <sup>4</sup> , Christopher Milne <sup>5</sup> , Jacinto Sá <sup>4,6</sup> , and Jakub Szlachetko <sup>1,\*</sup> 

- <sup>1</sup> Institute of Nuclear Physics, Polish Academy of Sciences, 31-342 Kraków, Poland; anna.wach@ifj.edu.pl (A.W.); joanna.czapla@ifj.edu.pl (J.C.-M.); rafal.fanselow@ifj.edu.pl (R.F.)
- <sup>2</sup> Department of Theoretical Chemistry and Biology, KTH Royal Institute of Technology, 10691 Stockholm, Sweden; delcey@kth.se
- <sup>3</sup> Paul Scherrer Institute, 5232 Villigen, Switzerland; christopher.arrell@psi.ch (C.A.); pavle.juranic@psi.ch (P.J.)
- <sup>4</sup> Department of Chemistry, Uppsala University, 75120 Uppsala, Sweden; marcus.lundberg@kemi.uu.se (M.L.); jacinto.sa@kemi.uu.se (J.S.)
- <sup>5</sup> European XFEL GmbH, 22869 Schenefeld, Germany; christopher.milne@xfel.eu
- <sup>6</sup> Institute of Physical Chemistry, Polish Academy of Sciences, 01-224 Warsaw, Poland
- \* Correspondence: wojciech.blachucki@ifj.edu.pl (W.B.); jakub.szlachetko@ifj.edu.pl (J.S.)

**Featured Application:** Herein, an innovative methodology, called X-ray chronoscopy, is proposed for exploration of ultrafast processes in matter with attosecond precision using current XFEL sources. The method is based on measuring the change in an X-ray pulse temporal profile induced by interaction with a medium.



**Citation:** Błachucki, W.; Wach, A.; Czapla-Masztafiak, J.; Delcey, M.; Arrell, C.; Fanselow, R.; Juranić, P.; Lundberg, M.; Milne, C.; Sá, J.; et al. Approaching the Attosecond Frontier of Dynamics in Matter with the Concept of X-ray Chronoscopy. *Appl. Sci.* **2022**, *12*, 1721. <https://doi.org/10.3390/app12031721>

Academic Editor: Emiliano Principi

Received: 10 January 2022

Accepted: 4 February 2022

Published: 8 February 2022

**Publisher's Note:** MDPI stays neutral with regard to jurisdictional claims in published maps and institutional affiliations.



**Copyright:** © 2022 by the authors. Licensee MDPI, Basel, Switzerland. This article is an open access article distributed under the terms and conditions of the Creative Commons Attribution (CC BY) license (<https://creativecommons.org/licenses/by/4.0/>).

**Abstract:** X-ray free electron lasers (XFELs) have provided scientists opportunities to study matter with unprecedented temporal and spatial resolutions. However, access to the attosecond domain (i.e., below 1 femtosecond) remains elusive. Herein, a time-dependent experimental concept is theorized, allowing us to track ultrafast processes in matter with sub-fs resolution. The proposed X-ray chronoscopy approach exploits the state-of-the-art developments in terahertz streaking to measure the time structure of X-ray pulses with ultrahigh temporal resolution. The sub-femtosecond dynamics of the saturable X-ray absorption process is simulated. The employed rate equation model confirms that the X-ray-induced mechanisms leading to X-ray transparency can be probed via measurement of an X-ray pulse time structure.

**Keywords:** X-ray free-electron laser (XFEL); X-ray chronoscopy; nonlinear X-ray-matter interaction; sub-femtosecond X-ray techniques

## 1. Introduction

Since the first discovery of X-rays, the field of X-ray studies has undergone a dramatic evolution, with new achievements and technological improvements. The present X-ray experiments are based on measuring X-ray energies and intensities of photons transmitted or emitted from matter. The dependencies on these two observable parameters are used to interpret physical, chemical and biological processes by means of X-ray diffraction, imaging, tomography and spectroscopy [1–3]. However, to capture the onset of the electronic changes in atomic species that drive matter transformations, observable parameters must be acquired with at least femtosecond temporal resolution as dictated by the core-hole lifetime [4–6].

X-ray free electron lasers (XFELs) have made available ultrashort X-ray pulses with peak brilliance, vastly exceeding those produced on third-generation light sources [7,8]. There are several demonstrations of sub-femtosecond XFEL pulses at extreme ultraviolet

(EUV), soft and hard X-ray wavelengths [9–12]. However, high photon flux density sources are needed, restricting usable sources to XFELs that deliver pulses of ca. 5 fs duration. It makes this unique light source among the fastest probes available for tracing transitions between different states of matter and providing access to fundamental physical, chemical, and biological processes. Nevertheless, the ultrashort XFEL pulses are still too long in the time domain to capture the first steps of electron dynamics in matter, e.g., onset of plasmon resonance process [13], visualization of Frank–Condon principle on complex systems [14], etc. Additionally, XFEL pulses have significant time jitter issues, making synchronization with optical pump pulses non-trivial and limiting even further temporal resolution in pump–probe experiments.

The time resolution limit may be bypassed by measuring the time profile of the incident and transmitted X-ray pulses, enabling time–domain experiments, called X-ray chronoscopy [15], and increasing the breadth of spectroscopic experiments at the XFEL. At the XFEL, the X-ray chronoscopy concept can be demonstrated with the help of terahertz streaking cameras [16–19], which allow for non-invasive temporal characterization of X-ray pulses with femtosecond and sub-femtosecond resolutions in different ways [10,11,18,20,21]. Our concept builds on the capabilities of the present terahertz streaking cameras to perform time–domain X-ray experiment, enabling XFEL experiments to approach the attosecond frontier [22,23].

A scheme of a conceptual X-ray chronoscopy experiment using terahertz (THz) streaking methods is depicted in Figure 1. The setup consists of two THz streaking detection systems with a sample placed between them. The detector upstream from the sample monitors the incident X-ray pulse temporal structure, while the downstream detector measures the transmitted X-ray pulse upon interacting with the sample material. With the described camera–sample–camera arrangement, the X-ray chronoscopic measurement is performed on a shot-to-shot basis, and the combined signals are then used to evaluate time-dependent phenomena related to the interaction of incidence X-ray pulse with the sample.

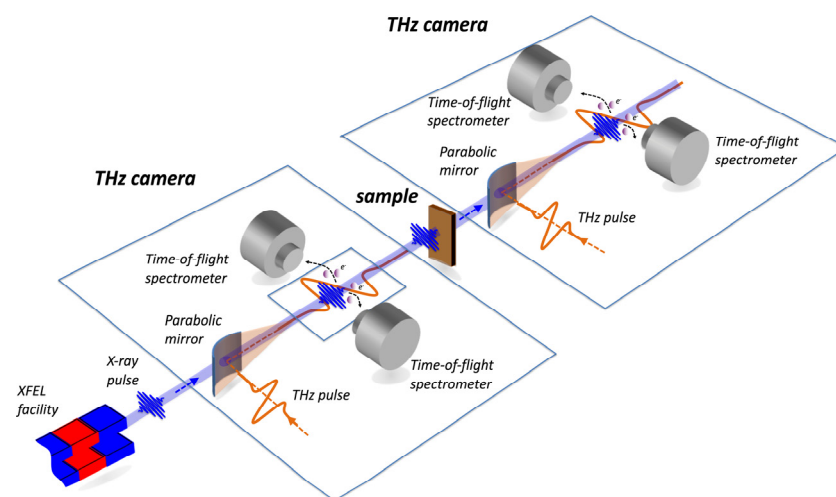


**Figure 1.** Schematic concept of X-ray chronoscopy experiment using two terahertz streaking spectrometers. The first THz setup is used to determine time distribution of the incident pulse ( $I_0(t)$  measurement), and the second one provides a measure of time distribution of X-ray pulse after interaction with the sample ( $I_1(t)$  measurement). Both spectrometers work in shot-to-shot mode, giving the possibility of either single-shot or cumulative measurement. The ratio of the measured time distribution curves will provide details on nonlinear processes induced by X-rays in the sample.

The relationship between the streaked photoelectron spectra and the complicated SASE pulse temporal structure has already been studied (see, e.g., Refs. [24,25]). Herein, we invoke the basis of terahertz streaking method and assess its capability to measure time-dependent X-ray pulse profiles at XFELs. Building on that, we theorize X-ray chronoscopy

capabilities to capture ultrafast electronic transitions dynamics. A saturable X-ray absorption process was used to demonstrate X-ray chronoscopy abilities to track dynamics during interaction between X-rays and matter. The simulated signals were compared to reported experimental results.

## 2. Materials and Methods

### 2.1. Principle of THz Streaking for Time-Dependent X-ray Pulse Analysis

THz and infrared streaking experiments have been used for nearly two decades to measure the temporal and spatial structure of high-harmonic generated (HHG) EUV pulses [22,23], and significant strides have been made to characterize soft X-ray pulse lengths at FEL facilities, e.g., at FLASH [17,18]. In addition, at the Linac Coherent Light Source (LCLS), Helml et al. used streaking experiments to measure the temporal structure of soft X-ray pulses directly in the time domain, and concluded that the shortest X-ray pulses available were no longer than 4.4 fs [26]. More importantly, they validated that the method is non-invasive, independent of photon energy, decoupled from machine parameters, and provides an upper bound on the X-ray pulse duration. The next step toward the method adaptation to hard X-ray FELs was the design of PALM (Photon Arrival and Length Monitor) at the SwissFEL, which was tested on HHG sources and the hard XFEL at SACLA [4,5,27].

The working principle of THz or IR streaking is based on the interaction of X-rays with a gas target, resulting in the generation of photoelectrons, which may gain or lose energy if the photoionization mechanism takes place in an external electric field. If the field amplitude is changing as a function of time, the energy change of the photoelectron from its normal photoionization energy is a way to establish when the electron was generated. The mapping of the temporal profile of the pulse to an electron energy spectrum can be approximated with the following equation [28]:

$$K_f = K_0 \pm \sqrt{K_0 U_p} \cos(\vartheta) \sin(\omega t), \quad (1)$$

where  $U_p = e^2 E_0^2 / (2m_e \omega^2)$  is the ponderomotive potential generated by the THz/IR beam,  $K_f$  and  $K_0$  are the final and initial kinetic energies of the electrons, respectively,  $\vartheta$  is the angle between the path of the electron and the polarization of the THz/IR beam,  $\omega$  is the angular frequency of the THz/IR pulse,  $t$  is time, and  $e$  and  $m_e$  are the electron charge and mass, respectively. For X-ray FEL pulses coming close to  $t = 0$ , the dependence of  $K_f$  on arrival time is nearly linear, with  $\Delta K = K_f - K_0 \approx \sin(\omega \Delta t)$  or  $\Delta K \approx s K_0 \Delta t$ , where  $s = dK/dT$  is the slope of energy versus time. Schematic principle of streaking of photoelectrons generated by X-ray pulse in a THz field is shown in Figure 2.

The restrictions on the method are that the X-ray temporal pulse length has to be shorter than the linear region around  $t = 0$ . For short pulses, as presented here, one could use 20–40 THz frequencies fairly easily, and if the jitter between the arrival time of the streaking field and the X-ray is small enough, one could even use 1600 nm wavelengths for the streaking effect. Such measurements have been performed already in laser laboratories [29], where the  $K_0$  from the HHG photoionization was fairly small and the accuracy was sub-100 as. With the schemes available for dealing with the likely arrival of a time jitter problem at XFELs [4,27], the path to sub-fs precision in hard X-ray pulse duration measurements is clear.

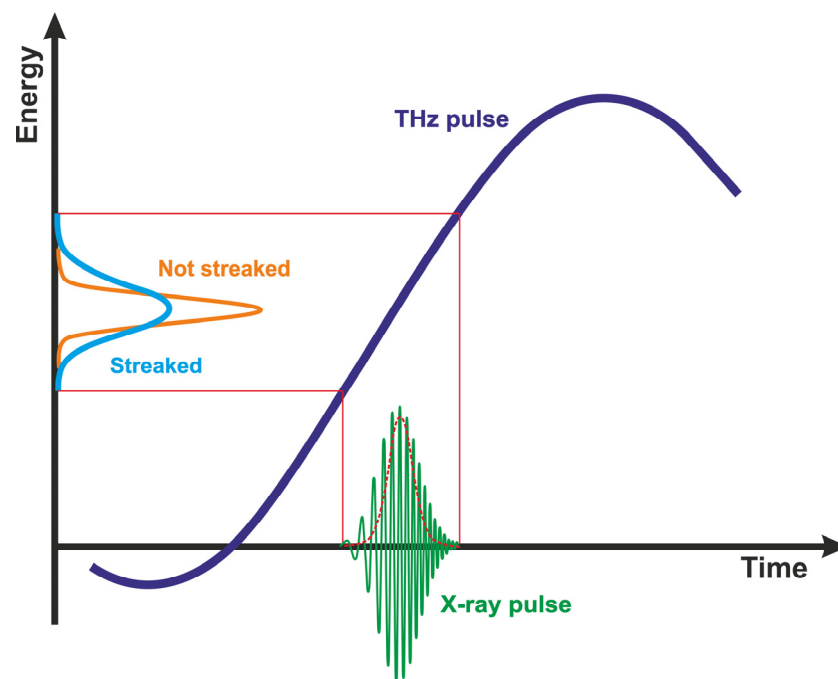


**Figure 2.** The streaking of an X-ray-induced photoelectron pulse in a THz vector potential. The X-ray pulse temporal profile is encoded in the energy spectrum of the measured photoelectron spectrum.

## 2.2. Time-Dependent Studies of Saturable Absorption at Hard X-ray Energies

Nonlinear spectroscopy has been studied theoretically and experimentally over decades in the optical domain [30] but has been made available recently at Ångström wavelengths due to the sharp increase in photon flux and short pulse duration provided by the XFELs [31]. Electronic states involved in X-ray-matter interaction have characteristic lifetimes extending to the sub-femtosecond domain, which is significantly shorter than the lifetimes expected for optical light-matter interaction processes. Furthermore, photoexcitation of a single core-level electron triggers a series of Auger transitions and electronic cascades lasting for a few femtoseconds. For this reason, the ultra-short X-ray pulses are necessary to overtake the Auger decays and to initiate nonlinear phenomena in the hard X-ray regime [32].

Historically, the first experiments devoted to X-ray-matter interactions at strong X-ray fields reported processes such as hollow-atom and high charge states formation [33] or plasma creation [34] as well as processes with low cross-sections such as two-photon absorption [35], stimulated X-ray emission [36] or X-ray-laser wave mixing [37]. In the present study, we focus on the saturable absorption (SA) mechanism, a first-order nonlinear process of interaction of X-rays with matter [38–40]. We deliberately chose this process as a case study for the X-ray chronoscopy method for several reasons. First, the incidence X-ray intensity required to initiate this process was already explored at XFELs, and the available experimental conditions are sufficient to initiate the SA process at every XFEL facility. Second, SA allows for a simple description of initial and final atomic configurations, and therefore the experimental data can be evaluated with known theoretical models and by employing developed theories dedicated to the electronic structure of many-electron systems.

The process of saturable absorption is the change of absorption properties of a material induced by the propagation of a strong laser beam. Such a process is a well-known phenomenon in laser technology at optical wavelengths, but it was only recently discovered in the X-ray regime due to the application of XFEL beams. Saturable absorption relates to the depletion of atomic ground-state species to the extent at which the sample becomes transparent to other photons of the same beam, i.e., there are no more absorbing states in

the system. In order to access such a regime, the X-ray ionization yields have to be higher than the decay rate transitions that allow the system to recover to the ground state.

The first experiment devoted to saturable absorption and to processes leading to sample transparency was performed on the L absorption edge of aluminum [40]. The experiment was executed at FLASH XFEL [41] and with 92.5 eV photons of the pulse duration of 15 fs at X-ray fluences up to 2 J/cm<sup>2</sup>. It was demonstrated that X-ray-induced transmission in the aluminum can be increased by up to 65% at the highest applied pulse fluences. From the experiment, it was concluded that the first part of the pulse ionizes L-shell electrons, and the created L-shell holes are filled at lower decay rates than ionization yields. The relatively long lifetime of the L-shell hole (40 fs) in aluminum allows for the strong depletion of L-states when using 15 fs X-ray pulse leading to the transparency increase.

At hard X-ray energies, the X-ray saturable absorption was detected for metallic Fe at the K absorption edge [38]. X-rays with energies around 7100 eV were used to monitor the change of the absorption coefficient over a 30 eV energy range. It was shown that in the regime of saturable absorption, the absorption coefficient is changing for both below- and above-edge energies. It was noted that changes were of opposite character, and an increase in the absorption coefficient was detected for below-edge energies. The experimental observation of saturable absorption effects could be explained with atomic kinetic simulations [39]. This has been demonstrated for solid-density aluminum plasma induced by XFEL pulses. It was shown that the absorption coefficient at the saturable absorption conditions has the opposite trend to that of the linear X-ray absorption spectrum. The effects of saturable absorption were also observed in our studies on an Fe<sub>2</sub>O<sub>3</sub> nanoparticle system in water solution [42]. It has been demonstrated that while the 1s core-hole lifetime is relatively short (below 1 fs) compared to the incidence pulse length (30 fs), the secondary processes and decay cascades are of importance for SA strength. Theoretical simulations confirmed that the return to the ground state after a single photoionization event is longer than the 35 fs-pulse length employed in the experiment.

### 3. X-ray Pulse Transmission in Saturable Absorption Conditions

The impact of saturable X-ray absorption on time distribution of photons in X-ray pulses penetrating elemental iron medium was examined, starting from the time-dependent Beer–Lambert law:

$$dI(x, t) = -I(x, t) \sigma n dx, \quad (2)$$

with  $I(x, t)$  denoting photon flux (number of photons per unit area and per unit time) at depth  $x$  and moment  $t$  (in cm<sup>-2</sup>s<sup>-1</sup>),  $\sigma$  is the interaction cross section (in cm<sup>2</sup>), dominated by the photoabsorption component at photon energy close to the K-shell binding energy, and  $n$  is the concentration of the target atoms (in cm<sup>-3</sup>). At a low intensity of the incident X-ray beam (low  $I(x, t)$ ), atoms have enough time to return to the ground state before arrival of another photon; thus, the atom concentration  $n$ , being effectively the concentration of capable absorbing centers, remains constant across the target depth and over the course of the pulse. At a higher intensity, atoms are excited with a higher rate, which makes a significant part of them unable to interact with many arriving photons. This phenomenon is referred to as saturable absorption. It necessitates consideration of a variable concentration of active absorbers  $n(x, t)$ , dependent on both  $x$  and  $t$  through the  $(x, t)$ -dependent photon flux and the dynamics of ground state reestablishment.

To account for the variable concentration of active absorbers  $n(x, t)$ , we employed a two-state picture of atom, with the ground state  $N_1$  and the excited state  $N_2$ . In this simple model, an atom in the ground state  $N_1$ , having absorbed a photon, is excited to the state  $N_2$ , and during the excited state lifetime  $\tau$ , it is unable to interact with photons. Once time  $\tau$  passes, the atom returns to the ground state  $N_1$  and is again capable of absorbing a photon. With this model, we describe the concentration of active absorbers  $n(x, t)$  as

$$n(x, t) = n_a N_1(x, t), \quad (3)$$



where  $n_a$  stands for the concentration of atoms in the target (in  $\text{cm}^{-3}$ ) and  $N_1(x, t)$ , a dimensionless value in the range (0,1), is the average ground state population per atom at depth  $x$  and moment  $t$ . With this relation, Equation (2) takes the following form

$$dI(x, t) = -I(x, t) \sigma n_a N_1(x, t) dx. \quad (4)$$

The population  $N_1(x, t)$  meets the relation

$$dN_1(x, t) = \left[ -I(x, t) \sigma N_1(x, t) + N_2(x, t) \frac{1}{\tau} \right] dt, \quad (5)$$

where the introduced  $N_2(x, t)$ , similar to  $N_1(x, t)$ , is a dimensionless value in the range (0,1) and denotes the average excited state population per atom at depth  $x$  and moment  $t$ . One can read from Equation (5) that  $N_1(x, t)$  decreases with the average number of photoabsorptions per atom (first summand) and grows with the average number of deexcitations per atom (second summand). With the condition  $N_1(x, t) + N_2(x, t) = 1$ , which ensures a constant number of available ground and excited states, Equation (5) can be rephrased in the following way

$$dN_1(x, t) = \left[ -\left( I(x, t) \sigma + \frac{1}{\tau} \right) N_1(x, t) + \frac{1}{\tau} \right] dt. \quad (6)$$

We simulated the influence of saturable X-ray absorption on time distribution of photons in an X-ray pulse using the system of Equations (4) and (6):

$$\begin{cases} \frac{dI(x, t)}{dx} = -I(x, t) \sigma n_a N_1(x, t) \\ \frac{dN_1(x, t)}{dt} = -\left( I(x, t) \sigma + \frac{1}{\tau} \right) N_1(x, t) + \frac{1}{\tau} \end{cases}. \quad (7)$$

The above system of differential equations for long lifetime  $\tau$  ( $1/\tau \rightarrow 0$ ) takes the form described in Ref. [43] and can be solved analytically for functions  $I(x, t)$  and  $N_1(x, t)$ , although the solutions are rather complicated. For the purpose of testing different parameters, including  $\tau$ , we developed a numerical algorithm capable of solving the above system of equations and determining tabulated  $I(x, t)$  and  $N_1(x, t)$  with arbitrary steps of time and length.

In the simulation, the target was 20  $\mu\text{m}$  thick iron foil spanning over  $0 \mu\text{m} \leq x \leq 20 \mu\text{m}$ . The parameters were chosen in order to verify the theoretical simulations with the reported experimental data [38]; thus, we used the X-ray pulse energy of 20  $\mu\text{J}$  and the cross-section value of  $3.73 \times 10^{-20} \text{ cm}^2$  for photoabsorption of 7130 eV photons [44]. Monochromatic X-ray pulses were assumed, thus neglecting the nonresonant excitations caused by the broad beam bandwidth as in [45,46]. For  $x \in [0 \mu\text{m}, 20 \mu\text{m}]$  the populations of initial states were  $N_1(x, t = 0) = 1$  and  $N_2(x, t = 0) = 0$ , and for other values of  $x$ , the populations were 0 at all moments. The time distribution of photons before interaction with the target, i.e.,  $I(x = 0 \mu\text{m}, t)$ , was described with a Gaussian with full width at half maximum (FWHM) of 7 fs. Despite the much more complex character of real time distribution of single XFEL pulses, the simplified Gaussian-like time envelope applied here suffice to evaluate the expected order of signal change. The excited state lifetime was given the value of 1 ns [47], thus distinctly longer than the typical XFEL pulse duration. A simulation was performed for a series of incident pulse intensities, with the time step  $dt$  of 0.05 fs and the path step size  $dx = c \times dt$  ( $c$ —speed of light in vacuum) of 0.015  $\mu\text{m}$ , as a smaller  $dt$  and  $dx$  resulted in an inefficiently long computation time. The speed of light entering the target medium was assumed to remain unchanged; thus, the refractive index was given the value of 1, and its change due to saturable absorption was not considered in the present analysis of pulse transmission. With the values of steps  $dt$  and  $dx$ , the transmission simulated for the low intensity of  $1.5 \times 10^9 \text{ W/cm}^2$  differed from the transmission calculated with the

Beer–Lambert equation by less than 2%, which we find reasonably low to illustrate the message conveyed in the present work.

The results of the simulation of the time-dependent X-ray pulse transmission are presented in Figure 3a for different incidence pulse intensities. When the incident pulse has low intensity (blue), linear absorption dominates, and as shown, it results in a constant transmission of about 0.0017 over the course of the pulse. The time distribution of the transmitted pulse preserves the Gaussian behavior of the incident pulse, scaled down by a constant factor, as shown in Figure 3b. In the high-intensity scenario (red), the transmission stays constant only until the moment of about 10 fs, when the photon flux, slowly rising on the Gaussian tail, is still relatively small. After that moment, the transmission undergoes a significant increase, resulting in the transmitted pulse time envelope considerably deviating from that of the incident pulse, including loss of the original Gaussian shape and shift in the time phase (i.e., shift of the pulse temporal center of mass). This effect results from saturable absorption of the photons arriving at earlier moments and turning the target transparent for the later arriving photons [40]. Figure 3a also contains two additional noisy datasets at the lowest and the highest intensities, which were simulated with stochastic SASE time envelopes. These datasets are temporal evolutions of transmission integrated over as few as 50 SASE pulses and precisely follow the chronoscopic signal simulated with Gaussian-like pulse profiles. Modification of time distributions of individual SASE-like pulses, shown in Figure 3c for the high- and low-intensity scenarios, has a similar tendency as for Gaussian-like pulses.

The linear attenuation coefficient  $\mu$  is empirically determined by measuring the radiation beam intensity before and after interaction with the target sample, and in a pulse-specific approach it can be calculated using the relation

$$\mu = \frac{-\ln\left(\frac{\int I_1(t) dt}{\int I_0(t) dt}\right)}{d} = \frac{-\ln(T)}{d}, \quad (8)$$

where the integration is performed over the range covering the entire pulse temporal envelope. The higher transmission  $T$  expected for higher incident intensity will be reflected in smaller measured values of  $\mu$ . Figure 4a presents the intensity dependence of the  $\mu/\mu_{\text{cold}}$  ratio, where the index “cold” refers to low incident intensity, i.e., to linear absorption conditions. As shown, the attenuation coefficient starts decreasing at intensities over  $10^{17}$  W/cm<sup>2</sup>, and the decrease strongly depends on the excited state lifetime. The saturation intensity, i.e., the intensity at which  $\mu = 0.5 \mu_{\text{cold}}$ , is above  $10^{19}$  W/cm<sup>2</sup>, grows with a decreasing lifetime. The saturation intensity grows much faster for lifetimes smaller than the pulse duration. Turning the iron foil transparent is illustrated in Figure 4b, showing hundreds-times increase in transmission in the intensity range studied. The results simulated using the simple two-level model described in this work correspond with the experimental and calculated data reported elsewhere [38]; however, a certain discrepancy can be observed that is not well understood due to the complexity of the decay dynamics at higher incident intensities. The discrepancy may be explained for example by the intense secondary Fe K $\alpha$  fluorescence radiation trapped in the sample, similar to the radiation trapping effect observed in the optical regime [48]. The K $\alpha$  radiation would resonantly sustain the excited state of the part of the iron atoms leading to the elongation of an effective excited state lifetime and turning the target transparent at an intensity lower than the one indicated by the calculations. The discrepancy might also originate from other ionization events occurring in parallel with the K-shell photoionization and initiated by the electron-impact ionization by the secondary photo- and Auger electrons. It has been shown that at high X-ray intensities, even with ultrashort XFEL pulses, a considerable fraction of Fe atoms probed via K $\beta$  decay had already interacted with the energetic electrons released through the photoionization of the atom’s surrounding [49]. It implies that at higher intensities, certain Fe atoms may have their M- and L-shells modified upon the incidence

of the 7130 eV-photon, which would make them incapable of K-shell photoionization and would boost the photoabsorption saturation.

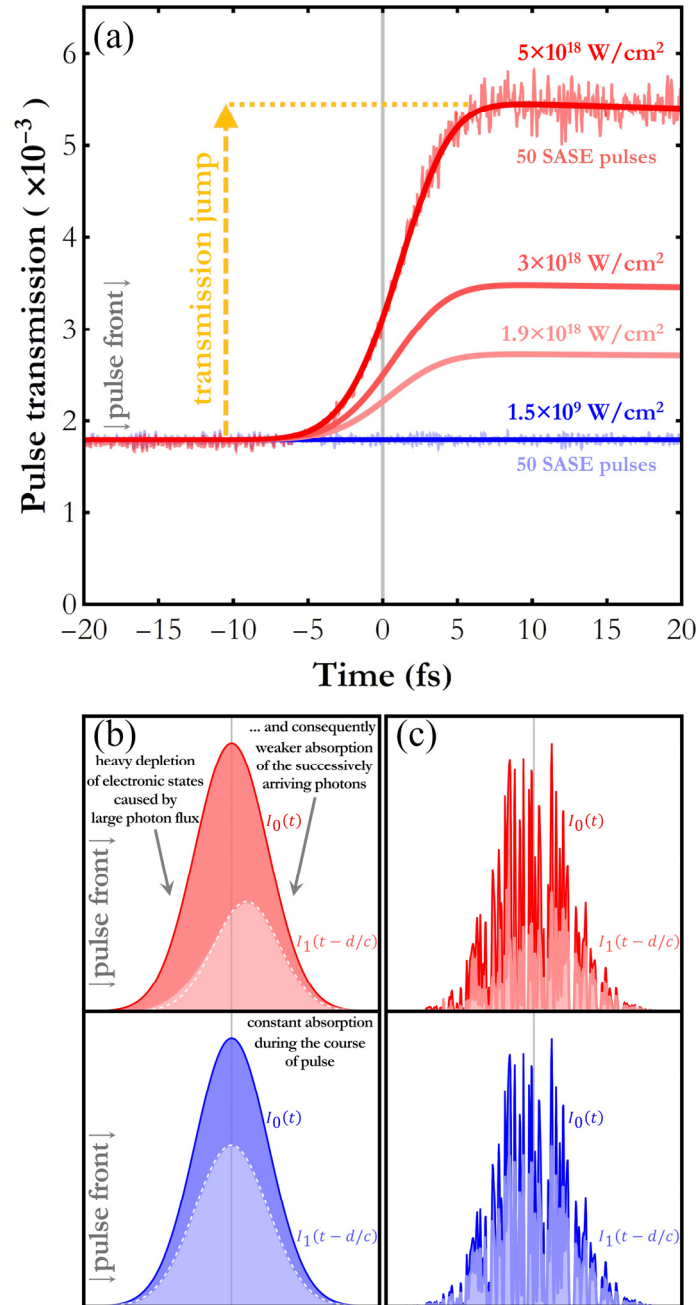


**Figure 3.** (a) Temporal evolution of transmission simulated for low- (blue) and high-intensity (red) pulses of 7130 eV photons through a 20  $\mu\text{m}$  thick Fe foil. Ratio  $I_1(t - d/c)/I_0(t)$  of time distributions of the transmitted pulse  $I_1(t) = I(x = d, t)$  and of the incident pulse  $I_0(t) = I(x = 0 \mu\text{m}, t)$ , with the target thickness  $d$  and the speed of light  $c$ , for different incident pulse average intensities  $\overline{I_0(t)} \times 7130 \text{ eV}$ . The plotted ratio shows the effect of pulse-target interaction on photon time distribution around the temporal center of mass of the incident pulse, hence the subtraction  $t - d/c$ . (b) Gaussian-like time envelopes  $I_0(t)$  and  $I_1(t - d/c)$  (not to scale) for low intensity (blue) and high intensity (red). Gaussian shape is delineated with the white dashed line. The transmitted pulse time envelope is shifted in time phase and loses the original Gaussian shape. (c) SASE-like time envelopes  $I_0(t)$  and  $I_1(t - d/c)$  (not to scale) for low intensity (blue) and high intensity (red).



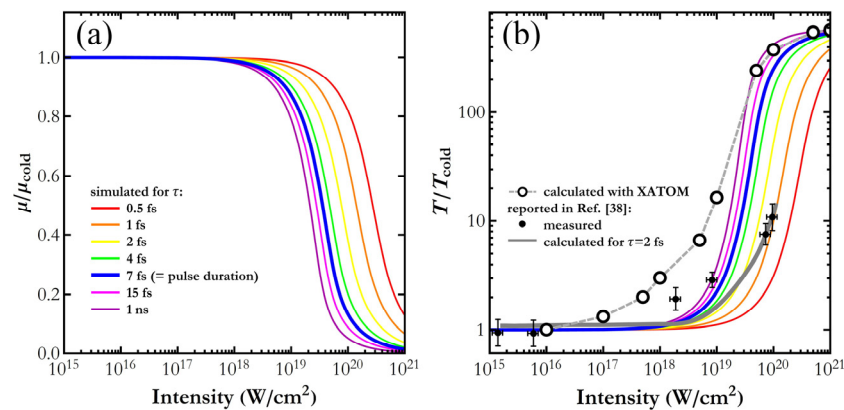


**Figure 4.** The influence of saturable absorption on linear attenuation coefficient (a) and transmission (b). (b) contains additional data taken from Ref. [38] measured and calculated for incidence X-ray pulse length of 7 fs as well as another dataset obtained with the XATOM code [50].

The transmission change calculated with the XATOM code considering such effects as photoionization, X-ray fluorescence decays, Auger and Coster–Kronig decays, elastic and Compton X-ray scattering as well as electron shake-off are also shown [50]. In the calculation, an isolated Fe atom was studied, which covered intra-atomic electronic transitions only. Thus, the electron recombination processes from the continuum were not accounted for, which is likely the primary cause of the transparency increase at an intensity lower than it was actually measured. In the X-ray flux range  $10^{17}$ – $10^{19} \text{ W}/\text{cm}^2$ , our two-level model underestimates the saturable absorption rates as compared to the XATOM results. It can be explained by the effect of competing photoionization and decay processes other than the K-shell photoionization, which are covered by the XATOM calculation, while in our model, only the K-shell photoionization is considered, as it is highly dominating over others (e.g., the ratio of partial photoionization cross sections  $\sigma_K/(\sigma_{L1}+\sigma_{L2}+\sigma_{L3}) \approx 9$  [44]). For X-ray fluxes above  $10^{19} \text{ W}/\text{cm}^2$ , the two models show a similar increase in the sample transparency as well as the photoabsorption saturation. Nevertheless, our model still well explains the experimental data.

#### 4. Summary

Herein, an innovative methodology, called X-ray chronoscopy, was proposed to access the attosecond frontier using the current XFEL pulses. The method is based on measuring the change of an X-ray pulse temporal profile induced by interaction with a medium. The concept of X-ray chronoscopy uses non-invasive terahertz streaking methodology to characterize the X-ray pulse time distribution with sub-femtosecond resolution [17,18]. The proposed approach requires two terahertz streaking camera setups arranged in the camera-sample-camera sequence to measure time distribution of the X-ray pulses incident on and transmitted through the sample. Through the analysis of the pulse temporal profiles measured before and after the sample, one can determine the evolution of the atomic-state populations and shell occupancies over the course of the pulse penetration through the medium. Note that many recent studies on nonlinear interactions report on the complexity of the measured data [27,33,51]. The reason is that often the nonlinear signal overlaps with the one resulting from linear X-ray-matter interaction, which in many cases, makes data analysis and interpretation unattainable. The proposed X-ray chronoscopy method, in its principle of operation, will not have this limitation. Any linear interaction of X-rays with matter will only be reflected as a constant component (i.e., absorption coefficient at a given energy) in the ratio of temporal X-ray beam profiles measured before and after the sample.

The concept of time-dependent measurements was investigated with a simple two-level model of saturable absorption in an elemental iron target for a series of intensities and the excited state lifetimes. The analysis showed that the saturable absorption leads to an increased transparency of the medium over the course of pulse propagation through

the target, and the saturation intensity depends on the material characteristics, such as the excited state lifetime, which agrees with the previously published data [38]. Finally, the saturable absorption leads to deformation of the X-ray pulse time distribution. The relative uncertainty, defined as the standard deviation of transmission at the pulse rear divided by the transmission jump (see Figure 3a), at the intensity of  $1.9 \times 10^{18} \text{ cm}^2$ , is expected to be around 6% for 50 incident SASE pulses. Based on the known XFEL performances and published THz streaking data, one can thus estimate that the X-ray chronoscopy experiment should be accomplished with good quality within a few hours by means of the proposed X-ray chronoscopy setup. Worth noting is the ongoing development of time diagnostics methods at XFELs, providing higher precision in temporal characterization of X-ray pulses and bringing X-ray chronoscopy closer to realization at XFELs. For instance, a pulse profile determination using a velocity map imaging (VMI) spectrometer has been demonstrated for attosecond soft X-ray pulses [10]. The fast, robust and simple derivation of pulse duration based on the center-of-energy shifts in the THz-streaked ionized electron spectra is also promising [21]. Precise pulse duration measurement before and after the target sample could be a prelude to realization of X-ray chronoscopy at XFELs.

**Author Contributions:** Conceptualization, W.B., J.S. (Jakub Szlachetko), C.A. and P.J.; methodology, W.B. and J.S. (Jakub Szlachetko); software, W.B., J.S. (Jakub Szlachetko), M.D., M.L. and J.S. (Jacinto Sá); validation, W.B., J.S. (Jakub Szlachetko), C.A. and P.J.; formal analysis, W.B. and J.S. (Jakub Szlachetko); investigation, W.B. and J.S. (Jakub Szlachetko); resources, all authors; data curation, W.B. and J.S. (Jakub Szlachetko); writing—original draft preparation, W.B., A.W. and J.S. (Jakub Szlachetko); writing—review and editing, all authors; visualization, W.B., A.W. and J.S. (Jakub Szlachetko); supervision, all authors; project administration, J.S. (Jakub Szlachetko); funding acquisition, J.S. (Jakub Szlachetko). All authors have read and agreed to the published version of the manuscript.

**Funding:** This work was supported by the National Science Centre (Poland) under grant No. 2017/27/B/ST2/01890.

**Institutional Review Board Statement:** Not applicable.

**Informed Consent Statement:** Not applicable.

**Data Availability Statement:** The calculated data presented in this work are available from the corresponding authors upon reasonable request. Figure 4b contains data available in Ref. [38].

**Conflicts of Interest:** The authors declare no conflict of interest. The funders had no role in the design of the study; in the collection, analyses, or interpretation of data; in the writing of the manuscript; or in the decision to publish the results.

## References

1. Bressler, C.; Chergui, M. Molecular Structural Dynamics Probed by Ultrafast X-ray Absorption Spectroscopy. *Annu. Rev. Phys. Chem.* **2010**, *61*, 263. [\[CrossRef\]](#) [\[PubMed\]](#)
2. Van Bokhoven, J.A.; Lamberti, C. *X-ray Absorption and X-ray Emission Spectroscopy*; John Wiley & Sons Ltd.: Hoboken, NJ, USA, 2016.
3. Renner, O.; Rosmej, F.B. Challenges of X-ray spectroscopy in investigations of matter under extreme conditions. *Matter Radiat. Extrem.* **2019**, *4*, 024201. [\[CrossRef\]](#)
4. Milne, C. SwissFEL: The Swiss X-ray Free Electron Laser. *Appl. Sci.* **2017**, *7*, 720. [\[CrossRef\]](#)
5. Gorgisyan, I. THz streak camera method for synchronous arrival time measurement of two-color hard X-ray FEL pulses. *Opt. Express* **2017**, *25*, 2080. [\[CrossRef\]](#) [\[PubMed\]](#)
6. Inoue, I. Atomic-Scale Visualization of Ultrafast Bond Breaking in X-ray-Excited Diamond. *Phys. Rev. Lett.* **2021**, *126*, 117403. [\[CrossRef\]](#) [\[PubMed\]](#)
7. McNeil, B.W.J.; Thompson, N.R. X-ray free electron lasers. *Nat. Photonics* **2010**, *4*, 814. [\[CrossRef\]](#)
8. Amann, J. Demonstration of self-seeding in a hard-X-ray free-electron laser. *Nat. Photonics* **2012**, *6*, 693. [\[CrossRef\]](#)
9. Huang, S.; Ding, Y.; Huang, Z.; Qiang, J. Generation of stable subfemtosecond hard X-ray pulses with optimized nonlinear bunch compression. *J. Phys. Rev. ST Accel. Beams* **2014**, *17*, 120703. [\[CrossRef\]](#)
10. Duris, J. Tunable isolated attosecond X-ray pulses with gigawatt peak power from a free-electron laser. *Nat. Photonics* **2020**, *14*, 30. [\[CrossRef\]](#)
11. Maroju, P.K. Attosecond pulse shaping using a seeded free-electron laser. *Nature* **2020**, *578*, 386. [\[CrossRef\]](#)

12. Malyzhenkov, A. Single-and two-color attosecond hard x-ray free-electron laser pulses with nonlinear compression. *Phys. Rev. Res.* **2020**, *2*, 042018. [[CrossRef](#)]
13. Rossi, T.P.; Erhart, P.; Kuisma, M. Hot-Carrier Generation in Plasmonic Nanoparticles: The Importance of Atomic Structure. *ACS Nano* **2020**, *14*, 9963. [[CrossRef](#)] [[PubMed](#)]
14. Condon, E.U. Nuclear Motions Associated with Electron Transitions in Diatomic Molecules. *Phys. Rev.* **1928**, *32*, 858. [[CrossRef](#)]
15. Bradley, D.J. Picosecond X-ray chronoscopy. *Opt. Commun.* **1975**, *15*, 231. [[CrossRef](#)]
16. Cavalieri, A.L. Clocking Femtosecond X-rays. *Phys. Rev. Lett.* **2005**, *94*, 114801. [[CrossRef](#)] [[PubMed](#)]
17. Frühling, U. Single-shot terahertz-field-driven X-ray streak camera. *Nat. Photonics* **2009**, *3*, 523. [[CrossRef](#)]
18. Grguraš, I. Ultrafast X-ray pulse characterization at free-electron lasers. *Nat. Photonics* **2012**, *6*, 852. [[CrossRef](#)]
19. Zhao, L. Terahertz Streaking of Few-Femtosecond Relativistic Electron Beams. *Phys. Rev. X* **2018**, *8*, 021061. [[CrossRef](#)]
20. Hartmann, N. Attosecond time–energy structure of X-ray free-electron laser pulses. *Nat. Photonics* **2018**, *12*, 215. [[CrossRef](#)]
21. Wieland, M. Deriving X-ray pulse duration from center-of-energy shifts in THz-streaked ionized electron spectra. *Opt. Express* **2021**, *29*, 32739. [[CrossRef](#)]
22. Hentschel, M. Attosecond metrology. *Nature* **2001**, *414*, 509. [[CrossRef](#)]
23. Drescher, M.; Hentschel, M.; Kienberger, R.; Tempea, G.; Spielmann, C.; Reider, G.A.; Corkum, P.B.; Krausz, F. X-ray Pulses Approaching the Attosecond Frontier. *Science* **2001**, *291*, 1923. [[CrossRef](#)] [[PubMed](#)]
24. Gorgisyan, I.; Ischebeck, R.; Prat, E.; Reiche, S.; Rivkin, L.; Juranić, P. Simulation of FEL pulse length calculation with THz streaking method. *J. Synchrotron Radiat.* **2016**, *23*, 643. [[CrossRef](#)] [[PubMed](#)]
25. Coffee, R.N.; Cryan, J.P.; Duris, J.; Helml, W.; Li, S.; Marinelli, A. Development of ultrafast capabilities for X-ray free-electron lasers at the linac coherent light source. *Philos. Trans. R. Soc. A* **2019**, *377*, 20180386. [[CrossRef](#)] [[PubMed](#)]
26. Helml, W. Measuring the temporal structure of few-femtosecond free-electron laser X-ray pulses directly in the time domain. *Nat. Photonics* **2014**, *8*, 950. [[CrossRef](#)]
27. Juranić, P.N. High-precision X-ray FEL pulse arrival time measurements at SACLA by a THz streak camera with Xe clusters. *Opt. Express* **2014**, *22*, 30004. [[CrossRef](#)]
28. Frühling, U. Light-field streaking for FELs. *J. Phys. B* **2011**, *44*, 243001. [[CrossRef](#)]
29. Gaumnitz, T.; Jain, A.; Pertot, Y.; Huppert, M.; Jordan, I.; Ardana-Lamas, F.; Wörner, H.J. Streaking of 43-attosecond soft-X-ray pulses generated by a passively CEP-stable mid-infrared driver. *Opt. Express* **2017**, *25*, 27506. [[CrossRef](#)]
30. Mukamel, S. *Principles of Nonlinear Optical Spectroscopy*; Oxford University Press: Oxford, UK, 1995.
31. Emma, P. First lasing and operation of an ångström-wavelength free-electron laser. *Nat. Photonics* **2010**, *4*, 641. [[CrossRef](#)]
32. Haynes, D.C. Clocking Auger electrons. *Nat. Phys.* **2021**, *17*, 512. [[CrossRef](#)]
33. Young, L. Femtosecond electronic response of atoms to ultra-intense X-rays. *Nature* **2010**, *466*, 56. [[CrossRef](#)] [[PubMed](#)]
34. Vinko, S.M. Investigation of femtosecond collisional ionization rates in a solid-density aluminium plasma. *Nat. Commun.* **2015**, *6*, 6397. [[CrossRef](#)] [[PubMed](#)]
35. Tamasaku, K. X-ray two-photon absorption competing against single and sequential multiphoton processes. *Nat. Photonics* **2014**, *8*, 313. [[CrossRef](#)]
36. Beye, M.; Schreck, S.; Sorgenfrei, F.; Trabant, C.; Pontius, N.; Schüßler-Langeheine, C.; Wurth, W.; Föhlisch, A. Stimulated X-ray emission for materials science. *Nature* **2013**, *501*, 191. [[CrossRef](#)] [[PubMed](#)]
37. Glover, T.E. Controlling X-rays with light. *Nat. Phys.* **2010**, *6*, 69. [[CrossRef](#)]
38. Yoneda, H. Saturable absorption of intense hard X-rays in iron. *Nat. Commun.* **2014**, *5*, 5080. [[CrossRef](#)]
39. Rackstraw, D.S. Saturable Absorption of an X-ray Free-Electron-Laser Heated Solid-Density Aluminum Plasma. *Phys. Rev. Lett.* **2015**, *114*, 015003. [[CrossRef](#)]
40. Nagler, B. Turning solid aluminium transparent by intense soft X-ray photoionization. *Nat. Phys.* **2009**, *5*, 693.
41. Bostedt, C. Experiments at FLASH. *Nucl. Instr. Meth. Phys. Res.* **2009**, *601*, 108. [[CrossRef](#)]
42. Kayser, Y. Core-level nonlinear spectroscopy triggered by stochastic X-ray pulses. *Nat. Commun.* **2019**, *10*, 4761. [[CrossRef](#)]
43. Parnis, J.M.; Oldham, K.B. Beyond the Beer–Lambert law: The dependence of absorbance on time in photochemistry. *J. Photochem. Photobiol. A* **2013**, *267*, 6. [[CrossRef](#)]
44. Schoonjans, T.; Brunetti, A.; Golosio, B.; del Rio, M.S.; Solé, V.A.; Ferrero, C.; Vincze, L. The xraylib library for X-ray–matter interactions. Recent developments. *Spectrochim. Acta Part B* **2011**, *66*, 776. [[CrossRef](#)]
45. Li, K.; Labeye, M.; Ho, P.J.; Gaarde, M.B.; Young, L. Resonant propagation of x rays from the linear to the nonlinear regime. *Phys. Rev. A* **2020**, *102*, 053113. [[CrossRef](#)]
46. Sun, Y.-P.; Liu, J.-C.; Wang, C.-K.; Gel'mukhanov, F. Propagation of a strong x-ray pulse: Pulse compression, stimulated Raman scattering, amplified spontaneous emission, lasing without inversion, and four-wave mixing. *Phys. Rev. A* **2010**, *81*, 013812. [[CrossRef](#)]
47. Durbin, S.M. X-ray pump optical probe cross-correlation study of GaAs. *Nat. Photonics* **2012**, *6*, 111. [[CrossRef](#)] [[PubMed](#)]
48. Sumida, D.S.; Fan, T.Y. Effect of radiation trapping on fluorescence lifetime and emission cross section measurements in solid-state laser media. *Opt. Lett.* **1994**, *19*, 1343. [[CrossRef](#)]
49. Blachucki, W. Inception of electronic damage of matter by photon-driven post-ionization mechanisms. *Struct. Dyn.* **2019**, *6*, 024901. [[CrossRef](#)]

- 
50. Jurek, Z.; Son, S.-K.; Ziaja, B.; Santra, R. XMDYN and XATOM: Versatile simulation tools for quantitative modeling of X-ray free-electron laser induced dynamics of matter. *J. Appl. Cryst.* **2016**, *49*, 1048. [[CrossRef](#)]
  51. Szlachetko, J. Establishing nonlinearity thresholds with ultraintense X-ray pulses. *Sci. Rep.* **2016**, *6*, 33292. [[CrossRef](#)]